Nanoscale

Accepted Manuscript

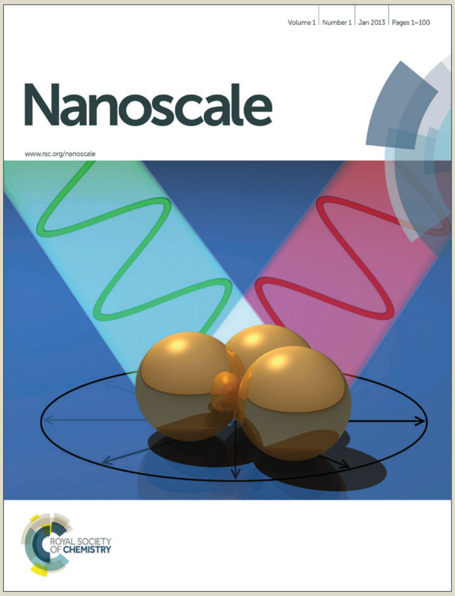

ROYAL SOCIETY OF CHEMISTRY

www.rsc.org/nanoscale

Journal Name

COMMUNICATION

B_{28}: smallest all-boron cage from *ab initio* global search†

Jijun Zhao,[a *] Xiaoming Huang,[a] Ruili Shi,[a] Hongsheng Liu,[a] Yan Su,[a] R. Bruce King[b]

Received 00th January 20xx,
Accepted 00th January 20xx

DOI: 10.1039/x0xx00000x

www.rsc.org/

Our *ab initio* global searches reveal a lowest-energy cage for B_{28}, which is built from two B_{12} units and prevails over the competing structural isomers such as planar, bowl, and tube. This smallest boron cage extends the scope of all-boron fullerene and provides a new structural motif of boron clusters and nanostructures.

Because of the short covalent radius, electron deficiency and flexibility to adopt sp^2 hybridization and three-center bonds, boron shows intriguing chemical bonding characteristics. In the past decade, boron clusters continue to surprise us by many unexpected novel structures, and thus have attracted significant attention [1-43].

In a pioneering *ab initio* study, Boustani [1] found that small boron clusters favor quasi-planar two-dimensional (2D) structures based on two fundamental units: pentagonal pyramidal B_6 and hexagonal pyramidal B_7. By comparing the simulated and measured photoelectron spectra, Wang, Boldyrev and co-workers showed that the anionic B_N^- clusters up to N=25 atoms are planar or quasi-planar [2-11]. For the neutral B_N clusters, the preference of quasi-planar geometries for N<20 has been confirmed by comprehensive *ab initio* calculations [12-14], whereas a structural transition from 2D to three-dimensional (3D) occurs at B_{20} which has a staggered double-ring tubular (DRT) configuration [3, 12, 15, 16]. Beyond B_{20}, double-ring or three-ring tubular (TRT) structures were believed to be the dominant motif up to at least 60 atoms [17, 18]. However, recent studies showed that some medium-sized clusters such as $B_{26\text{-}29}$ [19], B_{30} [20], B_{32} [21], B_{35} [22], and B_{36} [23] may adopt quasi-planar bowl-shaped configurations composed of networks of triangles stabilized with a central pentagonal, hexagonal, or heptagonal hole, which can be viewed as precursors to 2D extended boron sheets [24].

As an isoelectronic analogue of C_{60}, Yakobson's group [25] predicted a very stable B_{80} cage by adding one B atom in the center of all hexagonal facets of a B_{60} polyhedron. Inspired by the B_{80} cage with an optimal balance of triangles and hexagonal holes, a large variety of boron cages based on different construction rules have been proposed [17, 26-35]. However, *ab initio* global searches by our group [36, 37] and others [38-40] demonstrated that the core-shell structures centered by a B_{12} icosahedron as the precursors of bulk boron solids are more stable than the hollow cages for large B_N clusters with $N \geq 68$, mainly owing to the electron-deficient nature of boron that leads to higher coordination number for boron atoms [38].

Recently, there have been some breakthroughs in searching B_N cages in the medium size around N=40. Zhai et al. [41] reported experimental observation of a D_{2d} cage of B_{40} with an extremely low electron binding energy by photoelectron spectroscopy, which was further theoretically supported by unbiased global-minimum searches. A successive study by the same group identified a C_3 cage for B_{39}^- [42]. In an independent study using first-principles swarm structure search, Lv et al. [43] discovered a highly symmetric B_{38} fullerene-like structure (D_{2h}) with a large gap and high double aromaticity. These experimental and theoretical confirmations of all-boron fullerenes not only enrich the boron chemistry but also may lead to novel boron-based nanomaterials.

All of the above observations demonstrate strong competition between versatile structural motifs (e.g., hollow cage, double- or three-ring tubular, quasi-planar, core-shell) in the medium-sized boron clusters and reflect the intrinsically complicated nature of the potential energy surface (PES). Especially, the recent discovery of B_{38}, B_{39} and B_{40} cages brings up a critical question: what is the possibly smallest cage for a boron cluster as its ground state? In this communication, we carry out *ab initio* global searches revealing a new B_{12}-based motif for constructing boron cages. This leads to the ground state configurations for neutral and anionic B_{28} as well as possible cage structures for B_{26} and B_{27}.

Following our previous studies [36, 37, 44], an unbiased search on the PES of the neutral B_{28} cluster was carried out with a simulated annealing (SA) procedure incorporated with *ab initio* molecular dynamics (AIMD). The initial configuration of B_{28} was generated by random and heated up to 3000 K to remove possible memory effect. The time step of AIMD was 0.5 fs. Within the NVT ensemble, the system temperature was gradually annealed from 3000 to 300 K stepwise by 100 K decrements. At each temperature, AIMD

---

[a] Key Laboratory of Materials Modification by Laser, Ion and Electron Beams (Dalian University of Technology), Ministry of Education, Dalian 116024, China. E-mail: zhaojj@dlut.edu.cn
[b] Department of Chemistry and Center for Computational Chemistry, University of Georgia, Athens, Georgia, USA.

† Electronic Supplementary Information (ESI) available: Planar isomer structures of B_{28} and spatial distributions of front molecule orbitals. See DOI: 10.1039/x0xx00000x

simulation lasted for 15 ps at higher temperatures (1900-3000 K) and 25 ps at lower temperatures (300-1900 K), respectively. Hence, the total annealing time reached 580 ps. The final structure from SA-AIMD search was further refined by the basin hopping (BH) algorithm [45] also combined with *ab initio* calculations.

Table 1. Relative energy, HOMO-LUMO gap, vertical detachment energy (VDE), adiabatic detachment energy (ADE), binding energy (BE), and NICS for four representative B_{28} cluster isomers (shown in Figure 1). PBE0 optimizations on both neutral and anionic B_{28} clusters were done with the 6-311+G(d) basis set, while single-point energy CCSD(T) calculations were performed on the PBE0 geometries of neutral clusters with the def2-TZVP basis set.

	Relative energy (eV)			Gap (eV)	VDE (eV)	ADE (eV)	BE (eV/atom)	NICS (ppm)
	Neutral		Anion					
	PBE0	CCSD(T)	PBE0					
Cage	0	0	0	2.104	3.195	3.030	5.325	–38.3
Planar	0.034	0.029	0.182	2.489	3.020	2.874	5.323	–24.2
Tube	0.173	0.179	0.112	1.799	3.174	3.091	5.318	–38.8
Bowl	1.766	1.854	1.461	1.701	3.510	3.334	5.262	+5.8

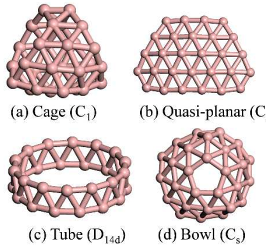

(a) Cage (C_1) (b) Quasi-planar (C_s)

(c) Tube (D_{14d}) (d) Bowl (C_s)

Figure 1. Isomer structures of B_{28} cluster belonging to different patterns: (a) cage, (b) quasi-planar, (c) tube, (d) bowl. For each structure, the symmetry is given in parenthesis.

A*b initio* calculations in both SA and BH searches were performed with density functional theory (DFT) with the plane-wave basis (400 eV cutoff energy) and ultrasoft pseudopotentials, as implemented in the VASP program [46]. The exchange-correlation interaction was described by the Perdew-Burke-Enzerhof (PBE) functional [47]. The cluster was placed in a large cubic supercell of 18 Å length to avoid interaction with its periodic images.

The final B_{28} structure from SA and BH searches, along with some candidate structures constructed for B_N clusters (N=26, 27, 28), were optimized using the PBE0 functional [48] and 6-311+G(d) basis set, as implemented in the Gaussian09 program [49]. Our previous benchmark calculations showed that both PBE and PBE0 are able to distinguish the structural isomers of B_{20} and give the correct energy order of the eight isomers compared to CCSD(T)/6-311G* results [34]. Vibrational analysis of these cluster isomers in their equilibrium configurations has also been carried out at the PBE0/6-311+G(d) level of theory to ensure that there are no imaginary frequencies corresponding to the saddle points on the PES. Finally, using the optimized PBE0/6-311+G(d) geometries, accurate single-point energy calculations were carried out on isomers of neutral B_{28} clusters using the CCSD(T) method and def2-TZVP basis set, as implemented in the ORCA program [50]. Excellent agreement of the relative energies is found between PBE0 and CCSD(T) calculations (see Table 1), further confirming that the PBE0 functional is reliable for distinguishing boron cluster isomers. Test calculations using different basis sets and PBE functional with the 6-311+G(d) were also performed and the results are given in Table S1 and S2 of the Supplementary Information. Within PBE0 functional, different basis give consistent energetic ordering of the four isomers in Figure 1, whereas PBE favors planar structure.

As displayed in Figure 1a, our global searches yield an unsymmetrical B_{28} cage consisting of thirty-six triangles, one hexagonal hole and two octagonal holes. According to previous analyses of 2D sheets as precursors of boron fullerenes [24], the three-center triangular units with unique three-center two-electron (3c-2e) bonding act as donors, while the hexagonal regions act as acceptors to accommodate the extra electrons. A neutral B_{28} cluster has a total of 84 valence electrons. Among them, 72 electrons are distributed on the 36 triangles for the 3c-2e bonds, while the remaining 12 electrons can be assigned to the three holes, probably four electrons for each hole.

Unlike the larger B_{38} and B_{40} cages with high symmetry [41, 43], 28 atoms in B_{28} are insufficient to form any symmetric cage with satisfactory balance between triangles and large holes. As a consequence, the optimal B_{28} cage shows no point-group symmetry (i.e., C_1). Even so, its HOMO-LUMO gap of 2.104 eV from PBE0 calculation is comparable to those of larger symmetric cages, i.e., 2.25 eV for B_{38} (D_{2h}) [43] and 3.13 eV for B_{40} (D_{2d}) [41], both calculated using the same PBE0 functional. The sizeable HOMO-LUMO gap of B_{28} cage can be related to its high stability.

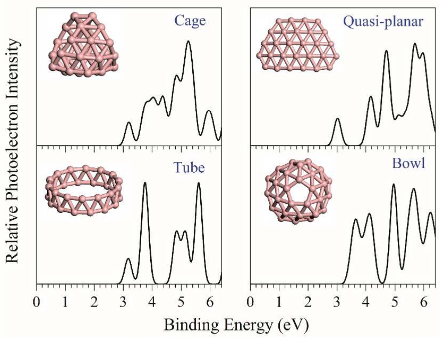

Figure 2. Simulated photoelectron spectra for selected B_{28} isomers (shown in insets) from PBE0/6-311+G(d) calculations. A uniform Gaussian broadening of 0.12 eV was adopted.

Figure 1 also depicts the geometries of other metastable isomers of B_{28}, including a quasi-planar sheet with a filled triangle network [19] (Figure 1b), a double-ring tube similar to B_{20} [3] (Figure 1b), and a bowl-like configuration with a central pentagonal hole like B_{30} [20] (Figure 1d). The relative energies and electronic properties of these four representative structures belonging to different motifs are summarized in Table 1. Previously, DRT was considered as the possibly lowest-energy configuration of B_N around N=28 [17, 18]. However, the C_1 cage from our global search prevails the DRT isomer by 0.173 eV at PBE0/6-311+G(d) level and 0.179 eV at CCSD(T)/def2-TZVP level, respectively. Meanwhile, the bowl-shape isomer of B_{28} is about 1.8 eV higher in energy, which is a consequence of the insufficient number of boron atoms to enclose the interior pentagonal hole, as compared to the C_{5v} bowl configuration of B_{30} [20].

The recently reported quasi-planar C_s structure of B_{28} [19] (Figure 1b) is slightly less favorable than the ground-state cage by ΔE = 0.034 eV (PBE) or ΔE = 0.029 (CCSD(T)). There are also many other possible (quasi-)planar isomers for B_{28} [19], which have been considered and presented in Figure S1 of the Supplementary Information. Interestingly, several planar isomers with one or two (pentagonal or hexagonal) holes, i.e., c, d, e, g, h in Figure S1, are substantially higher in energy than the hole-free sheet (Figure 1b) by over 0.79 eV, although they resemble the quasi-planar structures of B_{24}^- [9] and B_{25}^- [10]. Anionic boron clusters with an extra electron usually favor 2D configurations [16]. However, our PBE0/6-311+G(d) calculation demonstrates that the C_1 cage for B_{28}^- is more stable than the quasi-planar structure by 0.182 eV and the bowl structure by 1.461 eV. In other words, both neutral and anionic B_{28} clusters adopt the same 3D cage configuration as ground state. Our present finding of B_{28} cage, along with recent discoveries of quasi-planar B_{24} and B_{25}, bowl-shape B_{30}, B_{32} and B_{36} suggest strong competition between different structural motifs in the medium size range, making the global optimization of boron clusters even more intriguing and challenging.

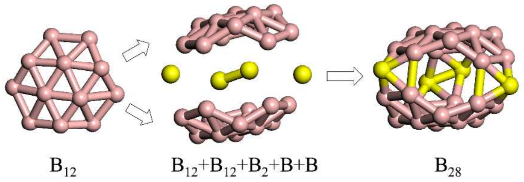

Figure 3. Routine for constructing the B_{28} cage from two quasi-planar B_{12} units and three linkers (B_2+B+B) highlighted in yellow.

Because of the correlation between atomic structure and electronic states, photoelectron spectroscopy is an efficient way to identify the lowest-energy configurations of anionic boron clusters [2-11, 22, 23, 41, 42]. To help experimentalists distinguish the isomers and identify the ground state structure, we simulate the photoelectron spectra of selected isomers for B_{28}^- cluster anion, as displayed in Figure 2. Distinctly different features of the photoelectron spectra are observed for various isomers. For instance, the VDE (3.195 eV) and ADE (3.030 eV) of the B_{28}^- cage are systematically higher than those of the quasi-planar C_s isomer of B_{28} (VDE = 3.020 eV, ADE = 2.874 eV) by about 0.2 eV. Moreover, there is a moderate gap (about 0.85 eV) between the first and second peaks in the photoelectron spectrum of B_{28}^- cage, whereas it is larger for the quasi-planar isomer (1.24 eV). All these differences should be sufficient for future experimental identification.

Previously, the stability of small planar or quasi-planar boron clusters [2, 39] and cages [34, 43, 44] has been partially attributed to aromaticity, which is associated with the extra stability arising from electron delocalization in complete circuits [51]. The nucleus independent chemical shift (NICS) can be used as a quantitative measure of aromaticity [52]. The PBE0/6-311+G(d) method computes NICS values at the centers for various cluster isomers in Figure 1 (Table 1). The B_{28} cage from our global search possesses an appreciable negative NICS value of about −38 ppm, suggesting that it is strongly aromatic. This is comparable to the previously reported NICS values for other boron cages, e.g., −21.9 ppm for B_{32} and −39.4 ppm for B_{44} [44], −50.7 ppm for B_{38} [43], −66.4 ppm for B_{76}, −44.8 ppm for B_{78}, and −24.7 ppm for B_{82} [34], respectively. A rough correlation between NICS values and relative energies is observed for the B_{28} isomers (Table 1). For instance, the metastable DRT isomer that is close to the ground state cage also has a large negative NICS value of −38.8 ppm, whereas the energetically unfavorable bowl-like structure is even anti-aromatic with a positive NICS value of +5.82 ppm. The electron delocalization in the B_{28} cage can be visualized by the frontier orbitals in Figure S2. The occupied frontier orbitals (HOMO, HOMO−1, HOMO−2) are distributed on both the triangles and the hexagonal/octagonal holes, whereas the unoccupied orbitals (LUMO, LUMO+1, LUMO+2) are mainly localized on the triangles.

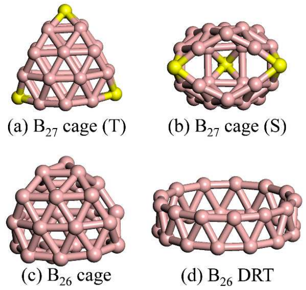
(a) B_{27} cage (T)
(b) B_{27} cage (S)
(c) B_{26} cage
(d) B_{26} DRT

Figure 4. Structures of B_{27} cage (a: top view, b: side view), (c) B_{26} cage, (d) B_{26} DRT. The three linker atoms in B_{27} are highlighted in yellow.

The present B_{28} cage can be built from two B_{12} clusters linked by two B atoms and one B_2 dimer, evenly enclosing three polygonal holes (Figure 3). According to previous studies [2, 4, 13], B_{12} with a quasi-planar convex structure (C_{3v}) is a unique doubly (σ- and π-) aromatic system. It possesses a large HOMO–LUMO gap of 2 eV, six delocalized π-electrons similar to benzene, and six σ-electrons that are responsible for delocalized global bonding between the three central B atoms and the nine peripheral B atoms. Hence the high stability of the B_{28} cage might be partly attributed to the very stable B_{12} building blocks. Such observations disclose a possible structural pattern for boron clusters and nanostructures with superstructures using smaller clusters such as B_{12} as building blocks. In this manner, we construct a symmetric B_{27} cages (D_{3h}) using two B_{12} units and three B linker atoms, as shown in Figure 4a and 4b. The binding energy of the neutral B_{27} cage is 5.310 eV/atom, rather close to that of B_{28} cage (5.325 eV/atom). However, its two-fold degenerate HOMO is only singly occupied with holes for three “missing” electrons. This suggests that neither the neutral nor the anionic B_{27} cage is chemically stable and corresponds to the ground state. However, the trianion, B_{27}^{3-} should be a stable species with a closed-shell electronic configuration. This further leads to prediction of an isoelectronic C_3B_{24} boron carbide cage via replacing three bridge B atoms by C, which has an exceptionally large HOMO-LUMO gap of 3.051 eV and an appreciable NICS value of −25.54 ppm.

Further removal of one bridge B atom in B_{27} leads to a C_1 cage of B_{26}, in which the two B_{12} units directly form B-B bonds (Figure 4c). However, geometry relaxations at the PBE0/6-311+G(d) level indicate the neutral B_{26} prefers a DRT structure (Figure 4d) rather than a C_1 cage with ΔE = 0.255 eV. Since both B_{26} and B_{27} clusters are unlikely to adopt cage configurations as their ground states, the B_{28} cage might be the smallest all-boron fullerene ever found. However, we cannot rule out the possibility of finding a quasi-planar structure of B_{28} with lower energy due to complexity of PES.

To summarize, our *ab initio* searches disclose a new all-boron cage for B_{28} that prevails the other structural motifs, including double-ring tube, bowl, quasi-planar triangle network. This B_{28} cage is composed of triangle facets uniformly doped with three polygonal holes, and can also be constructed from two highly stable B_{12} units. Both delocalized distribution of frontier orbitals and large negative NICS values (–38 ppm) show strong aromaticity that can account partially for the high stability. The present discovery of the possibly smallest boron cage at B_{28} extends the scope of all-boron fullerene and may stimulate further efforts on novel boron clusters and nanostructures with unusual structures and physical/chemical properties. We anticipate future experiments using photoelectron spectroscopy or other techniques to confirm our theoretical prediction.

This work was supported by the National Natural Science Foundation of China (11134005, 11304030).

Notes and references

1 I. Boustani, *Phys. Rev. B* 1997, **55**, 16426-16438.
2 H.-J. Zhai, B. Kiran, J. Li, L.-S. Wang, *Nat. Mater.* 2003, **2**, 827-833.
3 B. Kiran, S. Bulusu, H.-J. Zhai, S. Yoo, X. C. Zeng, L.-S. Wang, *Proc. Nat. Acad. Sci.* 2005, **102**, 961-964.
4 A. N. Alexandrova, A. I. Boldyrev, H.-J. Zhai, L.-S. Wang, *Coord. Chem. Rev.* 2006, **250**, 2811-2866.
5 A. P. Sergeeva, D. Y. Zubarev, H.-J. Zhai, A. I. Boldyrev, L.-S. Wang, *J. Am. Chem. Soc.* 2008, **130**, 7244-7246.
6 W. Huang, A. P. Sergeeva, H.-J. Zhai, B. B. Averkiev, L.-S. Wang, A. I. Boldyrev, *Nat. Chem.* 2010, **2**, 202-206.
7 Z. A. Piazza, W.-L. Li, C. Romanescu, A. P. Sergeeva, L.-S. Wang, A. I. Boldyrev, *J. Chem. Phys.* 2012, **136**, 104310.
8 A. P. Sergeeva, Z. A. Piazza, C. Romanescu, W.-L. Li, A. I. Boldyrev, L.-S. Wang, *J. Am. Chem. Soc.* 2012, **134**, 18065-18073.
9 I. A. Popov, Z. A. Piazza, W.-L. Li, L.-S. Wang, A. I. Boldyrev, *J. Chem. Phys.* 2013, **139**, 144307.
10 Z. A. Piazza, I. A. Popov, W.-L. Li, R. Pal, X. Cheng Zeng, A. I. Boldyrev, L.-S. Wang, *J. Chem. Phys.* 2014, **141**, 034303.
11 A. P. Sergeeva, I. A. Popov, Z. A. Piazza, W.-L. Li, C. Romanescu, L.-S. Wang, A. I. Boldyrev, *Acc. Chem. Res.* 2014, **47**, 1349-1358.
12 T. B. Tai, N. M. Tam, M. T. Nguyen, *Chem. Phys. Lett.* 2012, **530**, 71-76.
13 D. Y. Zubarev, A. I. Boldyrev, *J. Comput. Chem.* 2007, **28**, 251-268.
14 T. B. Tai, D. J. Grant, M. T. Nguyen, D. A. Dixon, *J. Phys. Chem. A* 2009, **114**, 994-1007.
15 W. An, S. Bulusu, Y. Gao, X. C. Zeng, *J. Chem. Phys.* 2006, **124**, 154310.
16 H. T. Pham, L. V. Duong, B. Q. Pham, M. T. Nguyen, *Chem. Phys. Lett.* 2013, **577**, 32-37.
17 C. Özdoğan, S. Mukhopadhyay, W. Hayami, Z. B. Güvenç, R. Pandey, I. Boustani, *J. Phys. Chem. C* 2010, **114**, 4362-4375.
18 F.-Y. Tian, Y.-X. Wang, *J. Chem. Phys.* 2008, **129**, 024903.
19 T. B. Tai, M. T. Nguyen, *Phys. Chem. Chem. Phys.* 2015, **17**, 13672-13679.
20 T. BaáTai, L. VanáDuong, H. TanáPham, D. T. TuyetáMai, M. ThoáNguyen, *Chem. Commun.* 2014, **50**, 1558-1560.
21 T. B. Tai, M. T. Nguyen, *Chem. Commun.* 2015, DOI: 10.1039/C5CC01252J.
22 Z. A. Piazza, H.-S. Hu, W.-L. Li, Y.-F. Zhao, J. Li, L.-S. Wang, *Nat. Comm.* 2014, **5**, 3113.
23 W.-L. Li, Q. Chen, W.-J. Tian, H. Bai, Y.-F. Zhao, H.-S. Hu, J. Li, H.-J. Zhai, S.-D. Li, L.-S. Wang, *J. Am. Chem. Soc.* 2014, **136**, 12257-12260.
24 H. Tang, S. Ismail-Beigi, *Phys. Rev. Lett.* 2007, **99**, 115501.
25 N. Gonzalez Szwacki, A. Sadrzadeh, B. I. Yakobson, *Phys. Rev. Lett.* 2007, **98**, 166804.
26 R. R. Zope, *Eurphys. Lett.* 2009, **85**, 68005.
27 Q.-B. Yan, X.-L. Sheng, Q.-R. Zheng, L.-Z. Zhang, G. Su, *Phys. Rev. B* 2008, **78**, 201401.
28 X.-Q. Wang, *Phys. Rev. B* 2010, **82**, 153409.
29 K. D. Quarles, C. B. Kah, R. N. Gunasinghe, R. N. Musin, X.-Q. Wang, *J. Chem. Theory Comput.* 2011, **7**, 2017-2020.
30 W. Hayami, S. Otani, *J. Phys. Chem. A* 2011, **115**, 8204-8207.
31 J. T. Muya, G. Gopakumar, M. T. Nguyen, A. Ceulemans, *Phys. Chem. Chem. Phys.* 2011, **13**, 7524-7533.
32 P. Boulanger, M. Morinière, L. Genovese, P. Pochet, *J. Chem. Phys.* 2013, **138**, 184302.
33 R. R. Zope, T. Baruah, K. C. Lau, A. Y. Liu, M. R. Pederson, B. I. Dunlap, *Phys. Rev. B* 2009, **79**, 161403.
34 S. Polad, M. Ozay, *Phys. Chem. Chem. Phys.* 2013, **15**, 19819-19824.
35 J. T. Muya, E. Lijnen, M. T. Nguyen, A. Ceulemans, *Chem. Phys. Chem.* 2013, **14**, 346-363.
36 J. Zhao, L. Wang, F. Li, Z. Chen, *J. Phys. Chem. A* 2010, **114**, 9969-9972.
37 F. Li, P. Jin, D.-e. Jiang, L. Wang, S. B. Zhang, J. Zhao, Z. Chen, *J. Chem. Phys.* 2012, **136**, 074302.
38 H. Li, N. Shao, B. Shang, L.-F. Yuan, J. Yang, X. C. Zeng, *Chem. Commun.* 2010, **46**, 3878-3880.
39 S. De, A. Willand, M. Amsler, P. Pochet, L. Genovese, S. Goedecker, *Phys. Rev. Lett.* 2011, **106**, 225502.
40 B. Shang, L.-F. Yuan, X. C. Zeng, J. Yang, *J. Phys. Chem. A* 2010, **114**, 2245-2249.
41 H.-J. Zhai, Y.-F. Zhao, W.-L. Li, Q. Chen, H. Bai, H.-S. Hu, Z. A. Piazza, W.-J. Tian, H.-G. Lu, Y.-B. Wu, Y.-W. Mu, G.-F. Wei, Z.-P. Liu, J. Li, S.-D. Li, L.-S. Wang, *Nat. Chem.* 2014, **6**, 727-731.
42 Q. Chen, W.-L. Li, Y.-F. Zhao, S.-Y. Zhang, H.-S. Hu, H. Bai, H.-R. Li, W.-J. Tian, H.-G. Lu, H.-J. Zhai, S.-D. Li, J. Li, L.-S. Wang, *ACS Nano* 2014, **9**, 754-760.
43 J. Lv, Y. Wang, L. Zhu, Y. Ma, *Nanoscale* 2014, **6**, 11692-11696.
44 L. Wang, J. Zhao, F. Li, Z. Chen, *Chem. Phys. Lett.* 2010, **501**, 16-19.
45 D. J. Wales, J. P. Doye, *J. Phys. Chem. A* 1997, **101**, 5111-5116.
46 G. Kresse, J. Hafner, *Phys. Rev. B* 1993, **47**, 558.
47 J. P. Perdew, K. Burke, M. Ernzerhof, *Phys. Rev. Lett.* 1996, **77**, 3865.
48 C. Adamo, V. Barone, *J. Chem. Phys.* 1999, **110**, 6158-6170.
49 M.J. Frisch, G.W. Trucks, H.B. Schlegel, G.E. Scuseria, M.A. Robb, J.R. Cheeseman, G. Scalmani, V. Barone, B. Mennucci, G. A. Petersson, *Gaussian 09, Revision A.01*. Editor, **2009**.
50 F. Neese, *Wiley Interdiscip. Rev.: Comput. Mol. Sci.* 2012, **2**, 73-78.
51 Z. Chen, R. B. King, *Chem. Rev.* 2005, **105**, 3613-3642.

52 P. v. R. Schleyer, C. Maerker, A. Dransfeld, H. Jiao, N. J. v. E. Hommes, *J. Am. Chem. Soc.* 1996, **118**, 6317-6318.